Installation Penalty of Aero-Engines on Narrow Body Aircraft

Boogaart, T.E.; Hoogreef, M.F.M.; Gangoli Rao, A.

Publication date
2022

Document Version
Final published version

Citation (APA)
Boogaart, T. E., Hoogreef, M. F. M., & Gangoli Rao, A. (2022). *Installation Penalty of Aero-Engines on Narrow Body Aircraft*. Paper presented at 33rd Congress of the International Council of the Aeronautical Sciences, ICAS 2022, Stockholm, Sweden.
https://www.icas.org/ICAS_ARCHIVE/ICAS2022/data/papers/ICAS2022_0246_paper.pdf

33RD CONGRESS
OF THE INTERNATIONAL COUNCIL
OF THE AERONAUTICAL SCIENCES
STOCKHOLM, SWEDEN, 4-9 SEPTEMBER, 2022

ICAS 2022 SWEDEN

INSTALLATION PENALTY OF AERO-ENGINES ON NARROW BODY AIRCRAFT

Thomas E. Boogaart[1], Maurice F.M. Hoogreef[1] & Arvind Gangoli Rao[1]

[1]Faculty of Aerospace Engineering, Delft University of Technology

Abstract

Decades of improvements of engine efficiency on internal engine components through better materials, design methods and novel fabrication techniques have resulted in fuel consumption reductions. Another major factor for improving engine fuel consumption has been the increase of bypass ratio. However, this has a significant impact on engine dimensions and weight, and, consequently, the installation of the engine on the airframe. Evaluation of engine installation penalties is not a new topic; literature provides various studies on aerodynamic effects. These primarily studied the effects of drag increase and the impact on drag of engine location and nacelle shape. This article investigates the performance impact of installation penalties from an increase in bypass ratio on narrow body aircraft, specifically the fuel consumption, weight and stability. Additionally, an analysis is made comparing aircraft retrofit and redesign for increased bypass ratio engines. It can be concluded from retrofit analyses that engine size is more significant than its location. Changes in aerodynamic center, C_{L_α}, and $C_{M_{AC}}$ cause stability/controllability criteria to shift to the left. Heavier engines at the same spanwise location cause a more forward CG location, which may become limiting. With the engine increasing in size (thus increasing the drag and increasing the weight), the overall increase in fuel burn is 5.9%. However, the decrease in fuel burn due when the SFC and engine effects are considered together, the fuel burn drops by 50%. The reduction in fuel burn thereby negating the increase in engine weight, drag, and integration issues. From BPR 10 onwards, the decreasing trend in tail size stagnates and actually reverses, indicating that larger tail sizes might be required for even larger BPR engines.

Keywords: engine installation penalties, aircraft design, aero-engine integration

Nomenclature

Latin Symbols

C_D	=	Drag coefficient ($\sim$)
C_L	=	Lift coefficient ($\sim$)
C_M	=	Moment coefficient ($\sim$)
S	=	Wing planform area (m^2)
S_h	=	Horizontal tail planform area (m^2)
W	=	Weight (N)

Acronyms

BPR	=	Bypass ratio
CG	=	Center of Gravity
CRM	=	Common Research Model
MTOM	=	Maximum Take-off Mass
NASA	=	National Aeronautics and
	=	Space Administration
OEM	=	Operative Empty Mass
SFC	=	Specific Fuel Consumption
TLAR	=	Top Level Aircraft Requirement
WB	=	Wing-body configuration
WBNP	=	Wing-body-nacelle-pylon
	=	configuration

1. Introduction

Emissions of greenhouse gasses by aviation have stimulated the governing bodies in the aviation sector to set ambitious goals to reduce CO2 and NOx emissions. Hence, making reduction of environmental impact one of the key focus areas of modern day aviation as, for example, illustrated by

the goals identified by the Air Transport Action Group[1] or the European Commission in its Flightpath 2050 [1] vision on aviation.

The best way to reduce the emissions is by burning less fossil fuels. Airlines themselves also have an incentive to reduce the fuel burn as the operation costs are directly correlated to the fuel burn. Hence it should not come as a surprise that in the last 70 years engine technology has made significant leaps. The, nowadays traditional, concept of tube and wing aircraft, where podded engines are typically wing-mounted has been widely adopted. These configurations allow easy accessibility for maintenance and noise shielding for the passengers. Early gas turbine powered civil aircraft, such as the Boeing 707, look very similar to the latest Boeing 737 MAX or Airbus A350. Over the years, engines have increased in diameter, primarily due to the increase in bypass ratio of the engine. An increase of bypass ratio results in a higher efficiency for thrust generation, with as a consequence that the diameter of the engine has to be increased. For example, the first generation 737 entered service in 1967, the latest 737 MAX in 2017 and both feature in principle the same airframe except for a newer, much larger diameter engine. The latter, because the rest of the airframe did not change, had to be relocated slightly. However, sufficient ground clearance is a problem and to solve this, the engine was moved forward and up. Consequently, impacting the pitching moment characteristics, due to the different location and much larger diameter (the nacelle becoming a more pronounced lift component as well).

An ideal aero-engine would have no weight, no drag and no exhaust flow while providing the required thrust through the centre of gravity of the aircraft. Unfortunately this is not possible. The engine does have a weight, an exhaust flow, and causes drag which all have an effect on the airframe performance. The following chapter describes the integration effects and the consequences on the aircraft design. An aircraft engine can be split into three main components: the gas generator, nacelle and pylon. Each component has a different effect on the aircraft and subsequently the aircraft performance. Figure 1 indicates the installation effect of the aforementioned components. The drag effects are indicated in red.

Previous research on engine installation penalties addresses the effect of engine location with respect to installation drag penalty [8, 11], where it was concluded that the optimal engine position yields a nearly constant installation drag coefficient for the lift range considered. Therefore, the authors concluded that the design goal should be to minimise the installation drag penalty for a given lift coefficient. Drag penalties were further detailed into the different components, such as pressure drag caused by the nacelle. Reducing the pressure drag for a gas turbine is very difficult as it is inherent to a body with thickness and curvature. The nacelle can be “streamlined”, thus reducing the wake size. The smaller wake reduces the pressure drag as well [10]. A better goal should be to avoid a rapid increase in pressure drag due to flow separation over the nacelle or in the inlet.

Another contribution of nacelle drag is related to spillage drag. Engine spillage drag is a different way of describing the profile drag of the nacelle. It is however associated with a drag increase due to off-design flight conditions. Spillage drag is defined by Covert as: the drag increase resulting from the difference between the inlet mass flow ratio at the operating conditions and the operating reference condition [5]. Aero engines operate at multiple, very different, flight- and operating conditions. Optimal would be the smallest possible inlet area for which no flow separation occurs in the inlet at take off thrust. Robinson [17] investigated the effect of engine geometry on spillage drag. The study was limited to a CFD analysis. The spillage drag was roughly 10% of the total drag calculated. The spillage drag was also dependent on the exhaust geometry used.

The nacelle, pylon and main wing are located closely together, causing a high likelyhood of local supervelocities, which may potentially lead to shockwaves (which should be avoided at all costs). Possible ways to reduce the chance of shocks are: increasing the distance between components or reducing local curvature. In the Boeing 777 engine study, the writers investigated the possibility of low velocity pressure side of the main wing to reduce local shock formation [3]. Alternatively, the nacelle shape can be modified to reduce supervelocities and reduce the chances of shockwaves.

The addition of the nacelle and pylon mounted to the main wing or fuselage means multiple bodies

[1] Air transport action group, Facts & Figures, May 2016, `https://www.atag.org/facts-figures.html`, visited on 7 June 2018

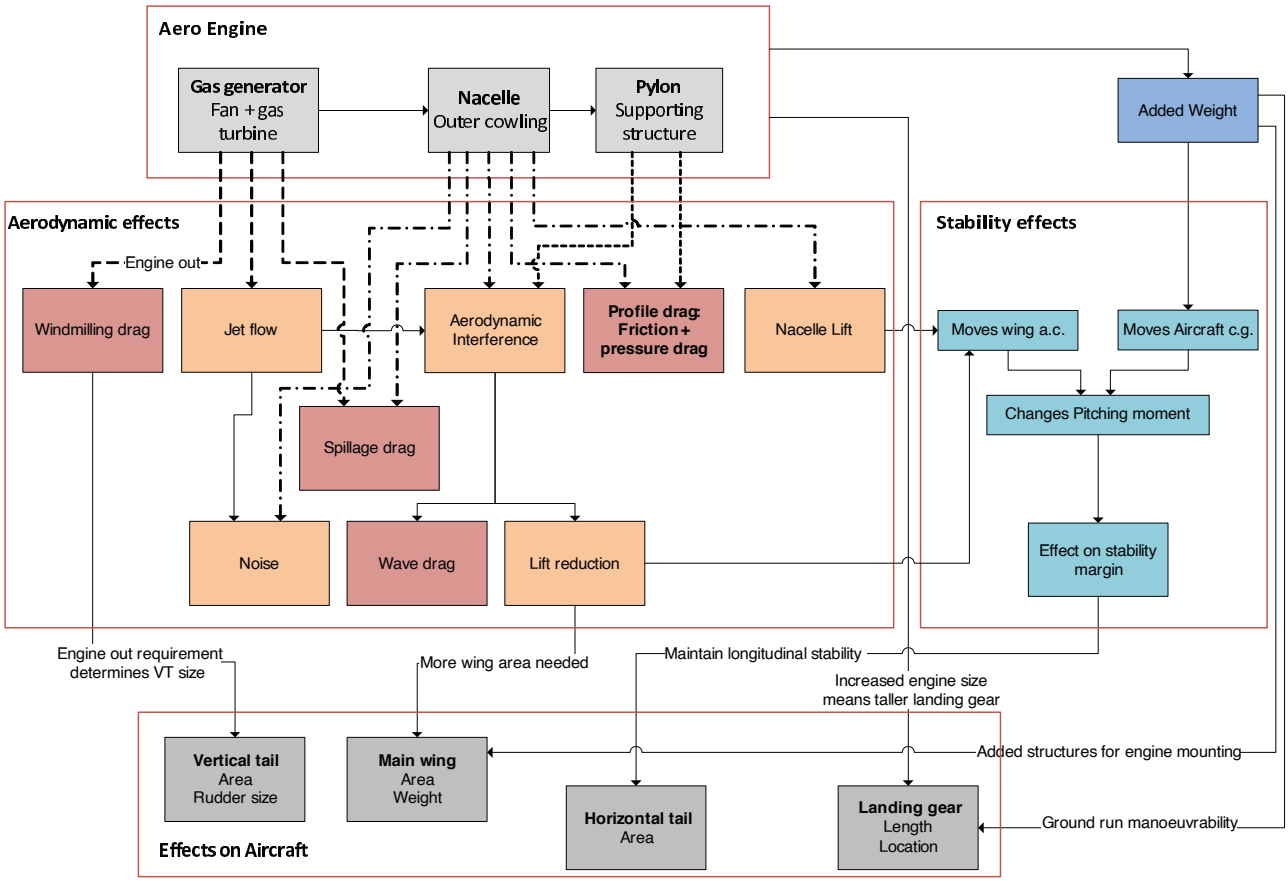

Figure 1 – Schematic of various installation effects, their dependencies and the consequences on the aircraft geometry

in close proximity. Interference between two bodies can be used as an advantage on lift generating bodies, e.g. multi-element flaps. For the pylon and nacelle it often results in an increase in drag and loss in lift [11, 21]. By moving the engine, the channels between the nacelle and wing can be altered to mitigate the interference effects. Hoheisel showed that with the engine installation there is a loss in lift on more than 60% of the span [11]. In general, when moving the engines more forward, the interference is reduced [3]. Engines moved more forward and keeping the same ground clearance, will result in a larger gully (the distance between the wing and nacelle) and reduced interference between nacelle and main wing. The loss of lift due to engines being present for low angles of attack means new trim conditions and possible higher trim drag compared to the aircraft without engines. According [18] increasing the vertical distance to the wing does not have a significant influence.

A special case of interference flows is caused by the exhaust flow. With under wing engines the jet flow moves over the pressure side of the wing, especially in case of far forward engines. The high velocity jet flow reduces the pressure on the bottom side of the wing and reduces the lift locally. Measures must be taken to ensure enough lift can be generated when the engines are installed [3]. Hoheisel showed that higher bypass ratio engines lead to smaller jet flow velocities due to better and more mixing of the exhaust gasses [11]. Although the effects of the jet flow are small, higher bypass engines are often located closer to the lower surface of the wing and as mentioned before this can have negative effects on the interference drag [15].

Engines located above and further behind the centre of gravity, the engines will have a stabilising effect [20]. If the engines are moved further back, the c.g. will move back as well. With the c.g. closer to the aerodynamic centre (a.c.), where the main lift vector acts, the required force by the tail will be reduced. With the engines moved back, the chance of higher interference drag becomes imminent. Another way to move back the c.g. is by moving the engines further outboard in case of a swept wing. However engines moved further outboard will yield directional stability problems in case of one-engine-out conditions [9]. For the Boeing 737 MAX the increased size of the LEAP 1B engine

caused stability problems. The larger bypass ratio meant a larger diameter of the nacelle and added weight. It also meant that in order to maintain the required ground clearance, the engines had to be moved forward to mount them higher. As a result, the aircraft had a nose up pitching moment for mid Mach numbers and high angles of attack [14].
Increasing the engine size will have an effect on the drag, weight and the aerodynamic performance (e.g. stability) of the aircraft. If space between the wing and the ground is limited, resulting in insufficient ground clearance, a redesign of the landing gear may be required, or a redesigned tailplane when engine thrust is increased. Quantifying, or at least getting a better understanding of the installation penalties, can provide new insights into the trade-off between an engine retrofit and a more drastic aircraft redesign. This may offer a basis for future aircraft and aero-engine design. If the installation penalties of a more efficient engine on an existing tube and wing airframe become too large, a new aircraft concept should be investigated. If retrofitting has no significant effect on the aircraft performance, it is still a worthwhile solution for current aircraft.

1.1 Paper objective

Trying to quantify all the installation penalties is quite a strenuous task, hence the objective of this article will be to investigate the impact of increased engine bypass ratio on aircraft designs, specifically on aircraft fuel consumption, weight and stability. The aim will be to identify the installation penalty of turbofan engines for engine retrofit on an existing airframe in terms of stability and controls, and the effects on fuel burn and required tail area for aircraft redesign, for single aisle narrow body aircraft.

1.2 Paper structure

The article will be structured in three main parts: (1) The method and validation, Section 2& Section 3, discussing the approach for retrofit analysis, aircraft sizing and validation of the aerodynamic solver. (2) Two sections on the results, Section 4, of the different studies on engine location, bypass ratio effects and effects of engine retrofits on existing aircraft, and Section 5.on the overall effect of integrating larger engines inside an aircraft design loop to perform a full aircraft resizing (taking into account the effects on size, mass and fuel consumption). The last part of the paper, (3), Section 6. provides the main conclusion to the research objectives.

2. Method

Two scenarios are illustrated in this article; (1) an engine retrofit scenario where a high by-pass ratio engines is fitted onto an existing airframe and (2) an aircraft re-sizing scenario where a complete aircraft design cycle is evaluated incorporating the high by-pass ratio engine. The following two subsections provide an overview of the approach that is used for each of the two scenarios.

2.1 Engine retrofit

Figure 2 schematically illustrates the approach of engine retrofit analysis. The engine retrofit analysis uses a baseline aircraft geometry (based on the Airbus A320-200) to compute the aircraft weight and center of gravity positions, using a Torenbeek [20] class-2 weight estimation. This information is combined with engine data from an engine database for various bypass ratios. The database consists of engines of different dimensions ranging from the CFM56 (found on the A320-200) to the CFM LEAP-1A, found on the A320NEO. The database is based on information from the ICAO aircraft engine emissions databank[2].
The aerodynamic analysis focuses on the evaluation of the retrofit scenarios by changing the dimensions and locations of the nacelle on an existing airframe. For the aerodynamic analysis, a vorticity-based potential flow solver is used to calculate the aerodynamic center location of the combined bodies. In viscous mode, the solution at the surface is used as a boundary condition for the viscous analysis. A validation of the solver is presented in 3.
Once the aerodynamic center is determined, the weight and balance of the aircraft, combined with aircraft geometry are added to perform a stability analysis. The latter is based on the so-called “scissor plot method” as detailed in the book by Torenbeek [20]. This relates longitudinal control and

[2] https://www.easa.europa.eu/domains/environment/icao-aircraft-engine-emissions-databank

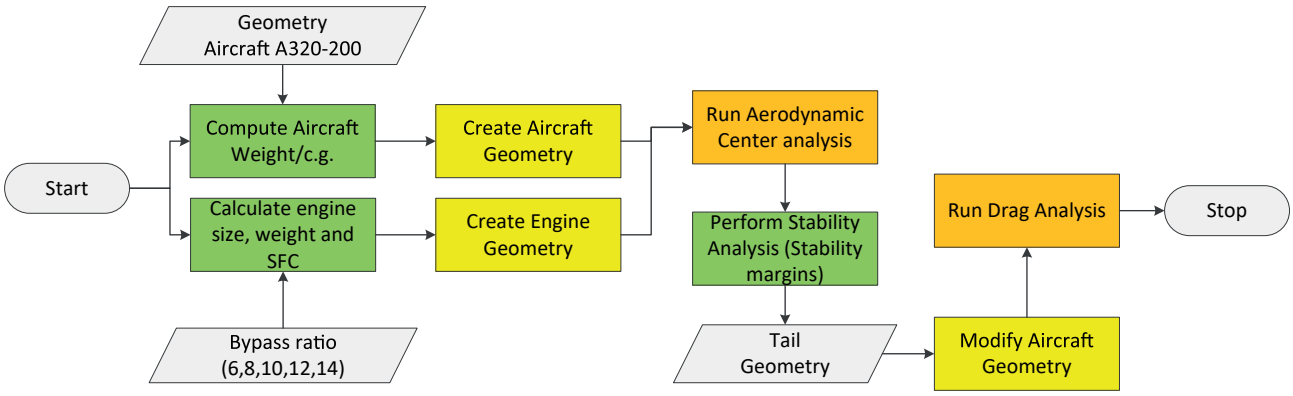

Figure 2 – Schematic of the engine retrofit analysis

stability requirements to the sizing of the stabilizing surfaces. The sizing methodology, often also referred to as a X-plot, uses the following stability and control constraints:

- Stick-fixed neutral points
- Control capacity required at stall
- Control capacity required at take-off rotation
- Control capacity required at landing flare-out

Using these constraints, the required horizontal tail area can be determined and this can be used to update the aircraft geometry and perform a (trim) drag analysis.

2.2 Aircraft (Re-)Sizing

Aircraft (re-)sizing is performed using the Aircraft Design Initiator (or in short the *Initiator*). It is a software tool developed in-house in Matlab. The software contains a design convergence loop over several disciplinary analyses, including handbook methods, empirical data and physics based methods. This software is capable of sizing both conventional and unconventional configurations (such as blended wing body aircraft and box-wing aircraft).
The Initiator was initially conceived as part of the European project Aerodesign (FP7) and has supported other European projects such as RECREATE (Horizon 2020) and Smart Fixed Wing Aircraft (Clean Sky). Currently, it is being used in NOVAIR (Large Passenger Aircraft framework) and CHYLA (thematic topic) under Clean Sky 2. The Initiator can be used to assess the impact of small and large changes to the aircraft on so-called key performance indicators.
The aircraft sizing process is explained in more detail in the article by Elmendorp et al. [7] and recent validation studies on various aircraft can be found in [12, 13, 23]. A flow chart of the sizing process is shown in Figure 3. The initiator performs a design convergence over a number of disciplinary analyses and sizing methods. The design convergence consists of three main convergence loops: a Class 2 loop, a Mission Analysis loop and a Class 2.5 loop.
The class 2 loop involves the basics of conceptual aircraft design, coupling a statistical weight estimation (Class 1 approach) to a constraint diagram analysis (wing-thrust loading diagram) in order to decide on the design point based on a set of top-level aircraft requirements (TLAR). This design point forms the starting point for a geometry estimation, primarily lifting surfaces and fuselage to fit the desired payload. This provides the input to a Class 2 weight estimation for which the method by Torenbeek [20] is used. An aerodynamic analysis (including drag estimation) concludes this loop.
The second loop performs a more detailed mission analysis, time-stepping through the mission profile and the horizontal stability estimation to size the tail surfaces required for stability and control according to the so-called scissor-plot method ([20], as used in the retrofit scenario as well. The Class 2.5 loop includes two semi-analytical weight estimation methods, a finite-element method based wing weight estimation [6] and a fuselage weight estimation [22] which is based on the method by Ardema et al. [2].

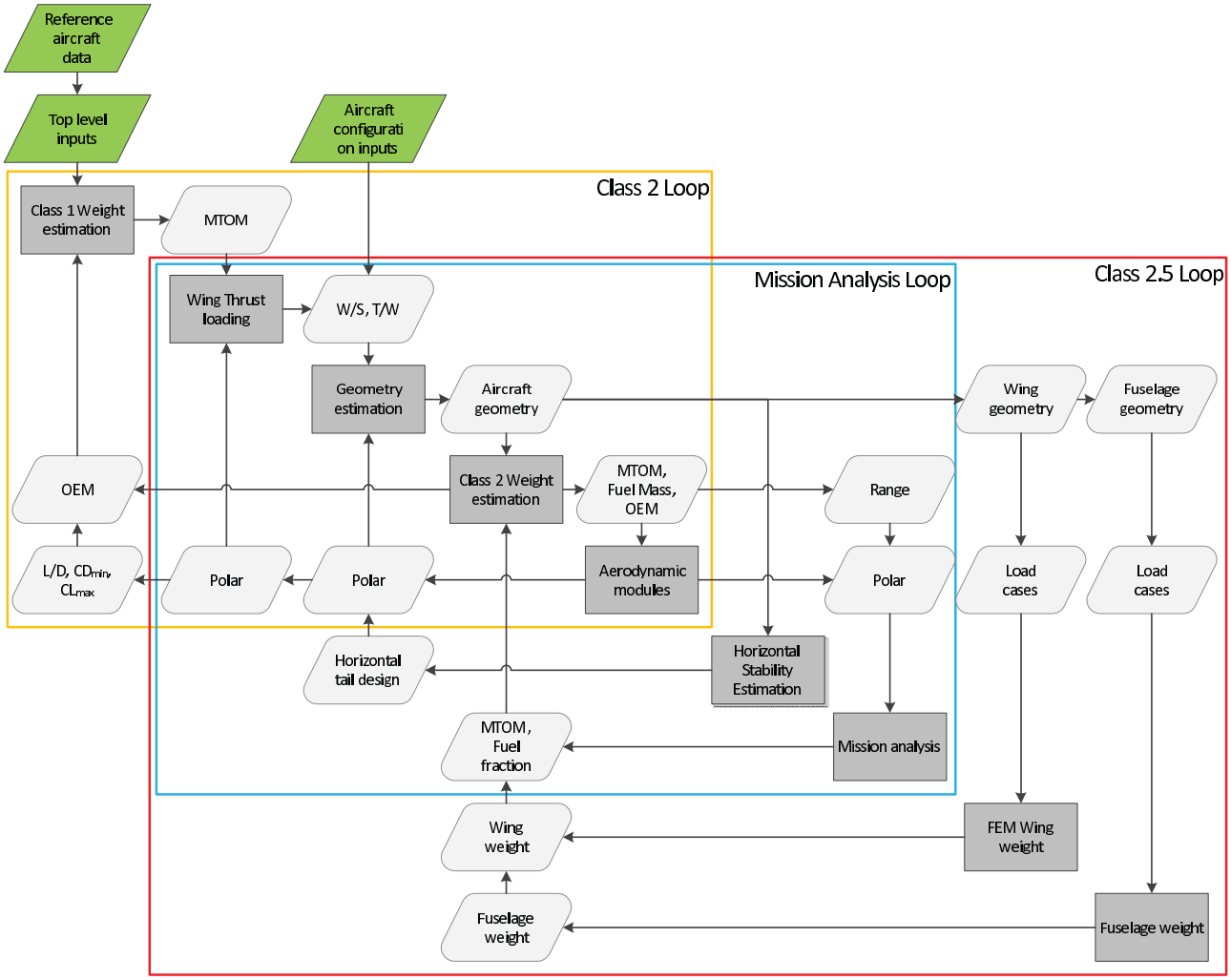

Figure 3 – Flow chart of the aicraft sizing process in the Aircraft Design Initiator

3. Validation of aerodynamic model

A validation study on the NASA common research model (CRM) from the 6th drag prediction workshop [19] has been performed. This is used to compare both wing body and wing body nacelle configuration with the vorticity solver that will be used to assess the impact of different size nacelles on the aerodynamics performance. This validation can be split into two main components; lift and drag prediction and pitching moment prediction. Validation with the FlightStream[3] surface vorticity solver was performed according to the same conditions as the experiment described by [16]. Solver settings are specified in Table 1 and uses the geometry of the scaled windtunnel model of CRM.

Table 1 – FlightStream settings used in the validation study.

Variable:	**Value**:
FlightStream version	2020.2
Lift/drag model	Pressure/Vorticity
Viscous drag model	Momentum integral
Moments model	Linear
Boundary layer type	Transitional
Flow separation	On
Compressibility correction	On

[3] `https://www.researchinflight.com/` - FlightStream 2020.2

3.1 CRM lift vs. drag prediction

The validation study results for lift and drag are presented in Figures 4 and 5 for the wing-body and wing-body-nacelle-pylon configurations, respectively. For the wing-body configuration in Figure 4, it can be observed that the lift-drag prediction is quite accurate except for the transition point and estimation of maximum lift coefficient. The transition from laminar to turbulent is a source of error when the results are compared to the experimental data. It becomes worse for the WBNP configuration.

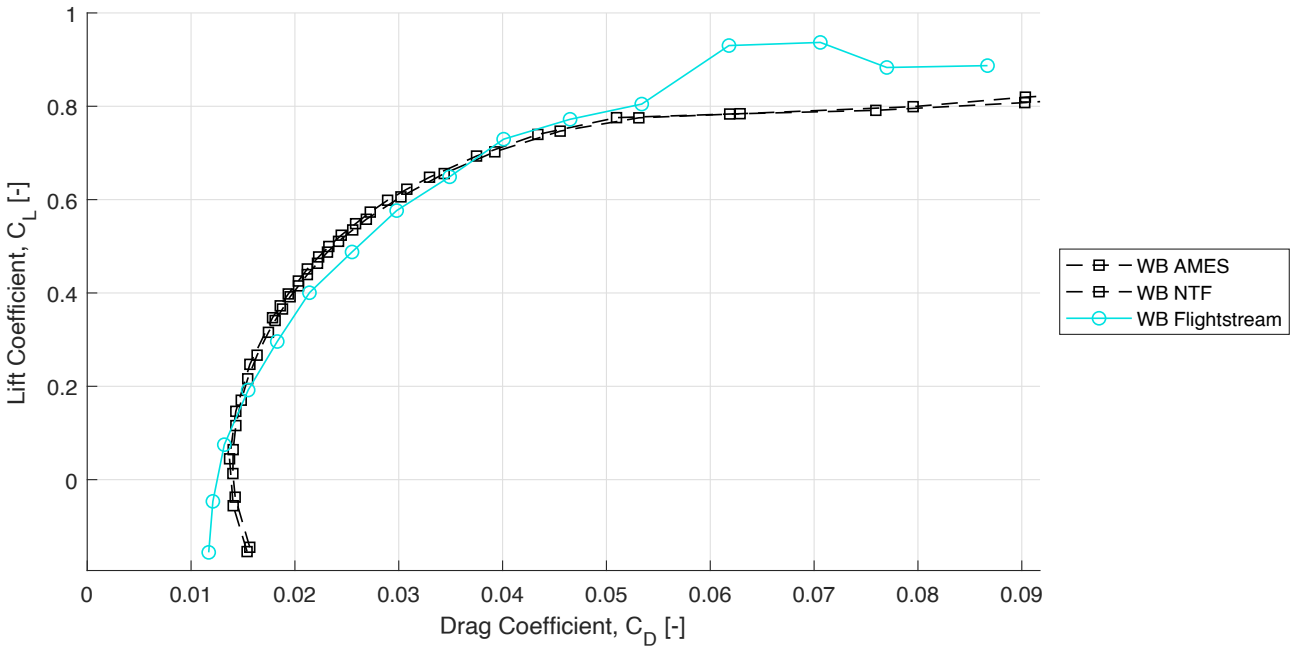

Figure 4 – Drag polar for CRM wing-body configuration with FlightStream results at Mach 0.7, Re 5 million, for the scaled model.

For the wing-body-nacelle-pylon configuration, the results in Figure 5 show the ability of the solver to capture the trends. However, both graphs show the limitations of a vorticity solver when calculating the drag coefficient. The viscous drag estimation is not sufficient to capture the correct values. For the WB configuration at lower lift coefficients the absolute values are of the same order of magnitude. At negative lift coefficients there is a large difference. Additionally, the slope of the FlightStream curve is different for the whole range compared to the experimental data.
The large drag increase after the separation is lacking. This is best visible for the WBNP case in Figure 5. For the WBNP configuration the drag is lower for all values of C_L, whereas the WB configuration showed a better estimation for the absolute values. The slope of the curve for the WBNP is closer to the experimental data.

3.2 CRM pitching moment prediction

The pitching moment calculated in FlightStream is shown in Figure 6. The absolute values for the pitching moment coefficient are different for the whole range of angles of attack. There is a trend that is captured for the WBNP configuration, since the slopes of both the FlightStream results and the experimental results are comparable. However, especially for small or negative angles of attack, there's a large difference between the magnitude of the results. Partially, this may be caused by the selected moment reference point.

3.3 Conclusions on CRM validation studies

Validation results on the NASA CRM have shown the capability to capture trends of lift, drag and pitching moment well, though typically with an underestimation of the magnitude of the latter two. For wing body combinations, result magnitudes are more accurate than when the nacelle is also included and match reasonable well (to the level that can be expected of such a solver). When flow separation starts, the difference increases. The pylon will be excluded as the meshing is delicate and the results

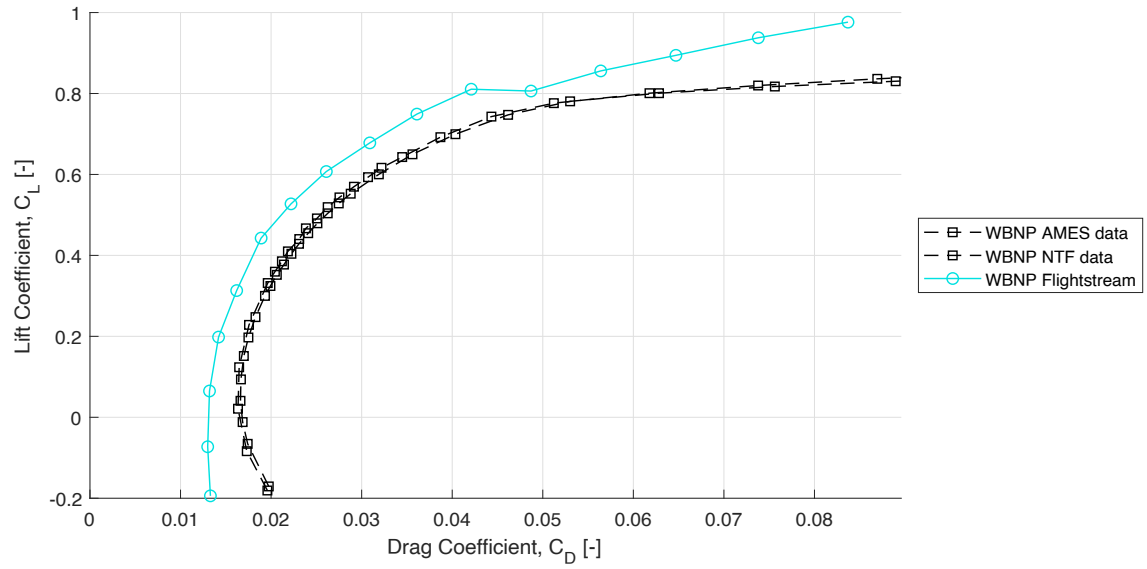

Figure 5 – Drag polar or CRM wing-body + nacelle and pylon configuration with FlightStream results at Mach 0.7, Re 5 million, for the scaled model.

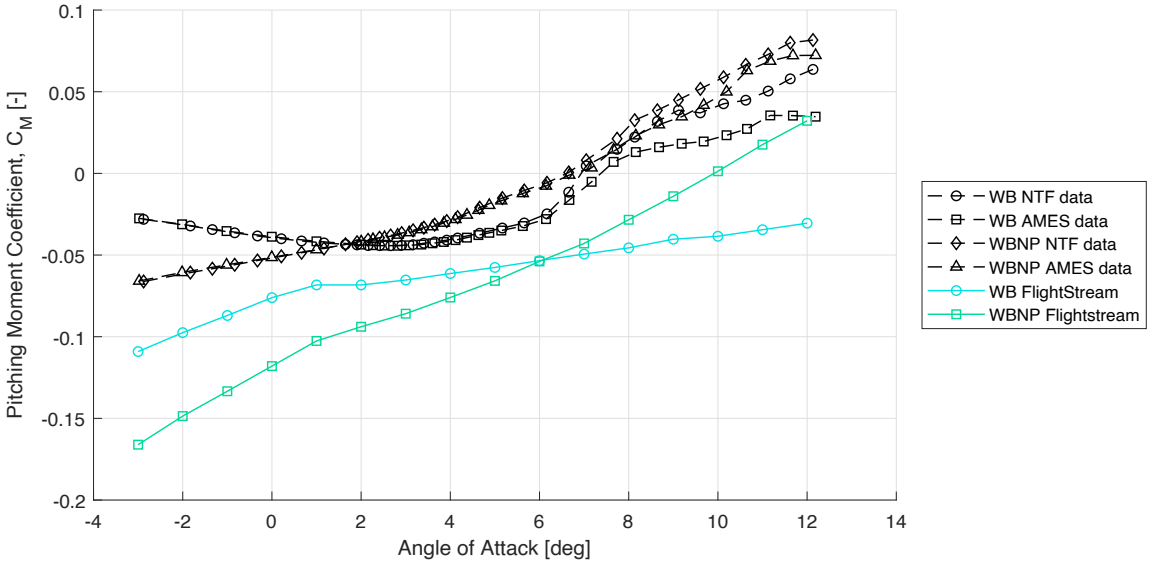

Figure 6 – Pitching moment for CRM configurations with FlightStream results at Mach 0.7, Re 5 million, for the scaled model.

are sensitive to changes in the mesh. A validation of the exclusions has shown that the impact of the pylon is minimal compared to the rest of the results. Comparing the drag polar from FlightStream for both configurations shows minimal differences, indicating that actually the software may not be able to properly capture the interference drag caused by the pylon (and nacelle) with the wing. Hence, omitting these is likely not going to impact the trends that are visible (which are properly captured) and it will also make sure that meshing problems of the pylon will not impact the results negatively.

4. Case study results for engine retrofit

Three cases are studied for the retrofit scenario, studying different locations and dimensions of the engines, as illustrated in Figure 7, top to bottom. These include: (1) keeping the engine location constant but changing the engine size (Case 1), (2) constant spanwise engine location and (3) moving vertical and spanwise location. Hence, the following sets of constraints are defined:

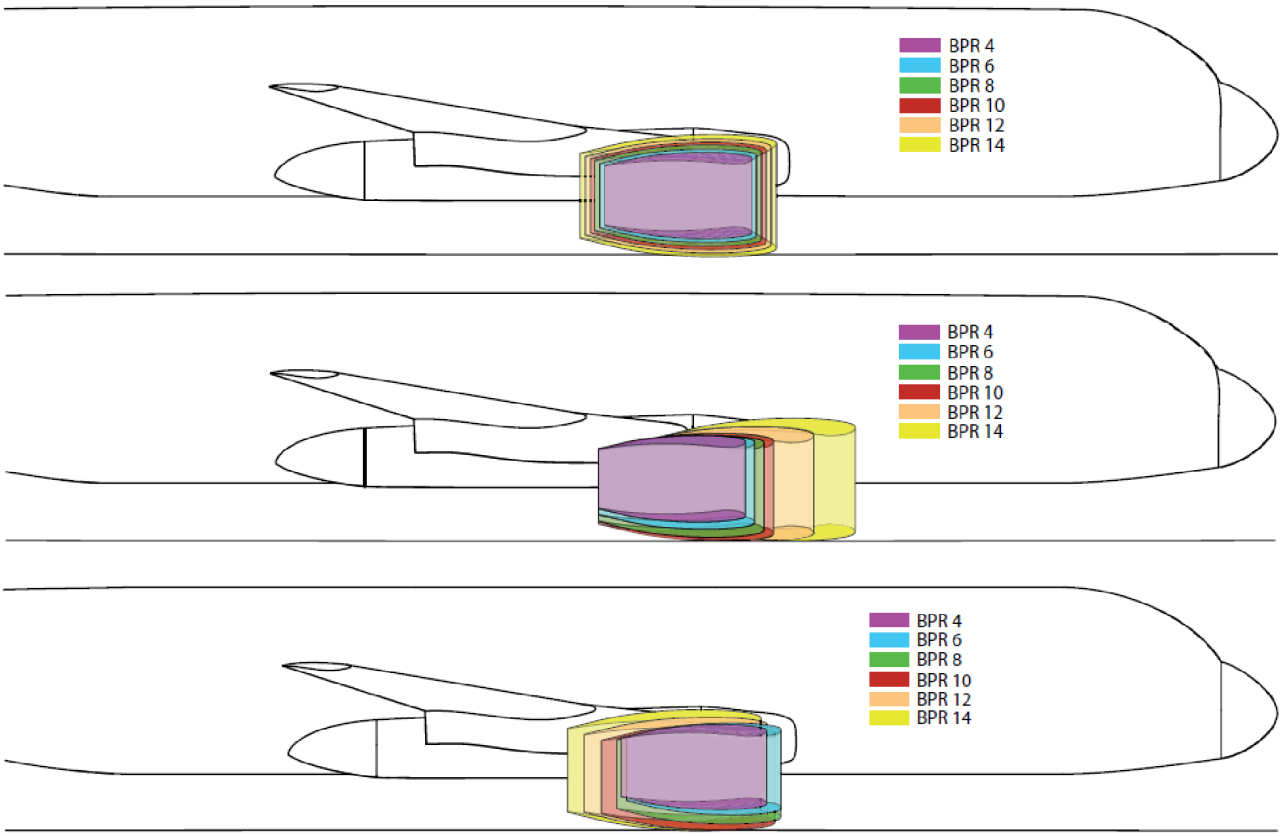

Figure 7 – Illustration of the case studies performed for the retrofit scenario. Top to bottom: case 1 - change engine size, case 2 - constant spanwise location and change vertical location & case 3 - change vertical and spanwise location

Case 1:

1. Keep engine location the same, but change engine size only

Case 2:

1. Keep gully distance the same.
2. Keep spanwise location the same.
3. Move larger engine down to a minimum ground clearance (The LEAP1-A engine is used as a guidance).
4. Move engine forward and up.

Case 3:

1. Keep the aircraft centre of gravity the same by correcting for engine weight.
2. Keep gully distance the same.
3. Move larger engine down to minimum ground clearance (The LEAP1-A engine is used as a guidance).
4. Move engine outboard and forward maintaining the gully distance.

4.1 Effect of engine location

Prior to investigating the different cases, an analysis is made of the relative effect of engine location on the aerodynamic center location. This analysis is shown in Figure 8 and Figure 9 for cruise and landing conditions, respectively. In both figures the relative change with respect to the baseline engine position is shown for the CFM56 and LEAP-1A engines. Negative values mean that the aerodynamic center moves forward with respect to the original position along mean aerodynamic chord.

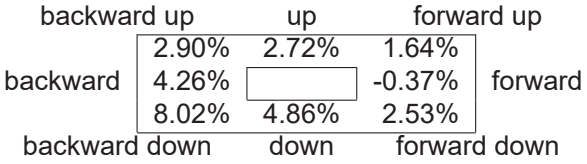

(a) Cruise condition CFM56

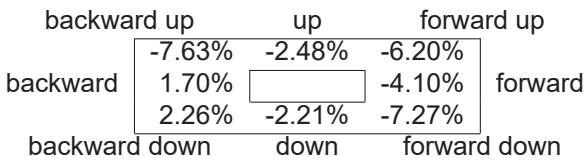

(b) Cruise condition LEAP-1A

Figure 8 – Comparison of the a.c. location for the A320 airframe with CFM56 and Leap-1A type engine. Evaluated at different locations (percentile change w.r.t reference value), at cruise condition.

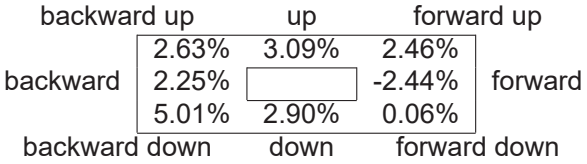

(a) Landing condition CFM56

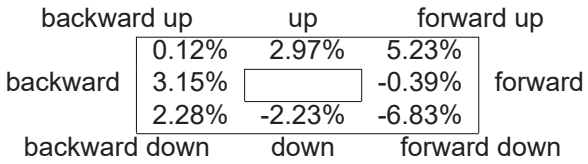

(b) Landing condition LEAP-1A

Figure 9 – Comparison of the a.c. location for the A320 airframe with CFM56 and Leap-1A type engine. Evaluated at different locations (percentile change w.r.t reference value), at landing condition.

It can be seen that moving the engine has a much more significant effect for the larger bypass ratio engine. In fact, where the directions of aerodynamic center shift are similar (though different magnitude) for the CFM56, they can be opposite and of significant difference in magnitude for the LEAP-1A. This indicates that in fact, the engine size may be more significant than its location. Though it must be noted that the effect on CG due the engine shift is not taken into account here. Additionally, it can be concluded that interference effects between the nacelle and wing have a significant effect that cannot be predicted when evaluating both individually.

4.2 Effect of bypass ratio

This subsection shows the effect of engine bypass ratio, by studying the different stability/controllability X-plots for the most extreme conditions of BPR 4 and 14. These effects are studied for all three cases where engine position and size can be varied according to the description earlier in this section.

Case 1:

The effect of increasing BPR for Case 1 (only changing engine dimension, not its location) is shown in Figure 10. The most obvious effect is the change in CG excursion, which has shifted forward together with both controllability lines. The larger engine is heavier, causing a more forward CG location. Inspecting the stability lines also reveals a shift to the left. The graph indicates that the tail area could be reduced (similar to the baseline condition, yet the reference tail surface is impacted by the A320's family design, i.e. it being sized for the A318). However, there is a restriction in the sense that the wing should also be moved forward due to the limiting forward CG position.

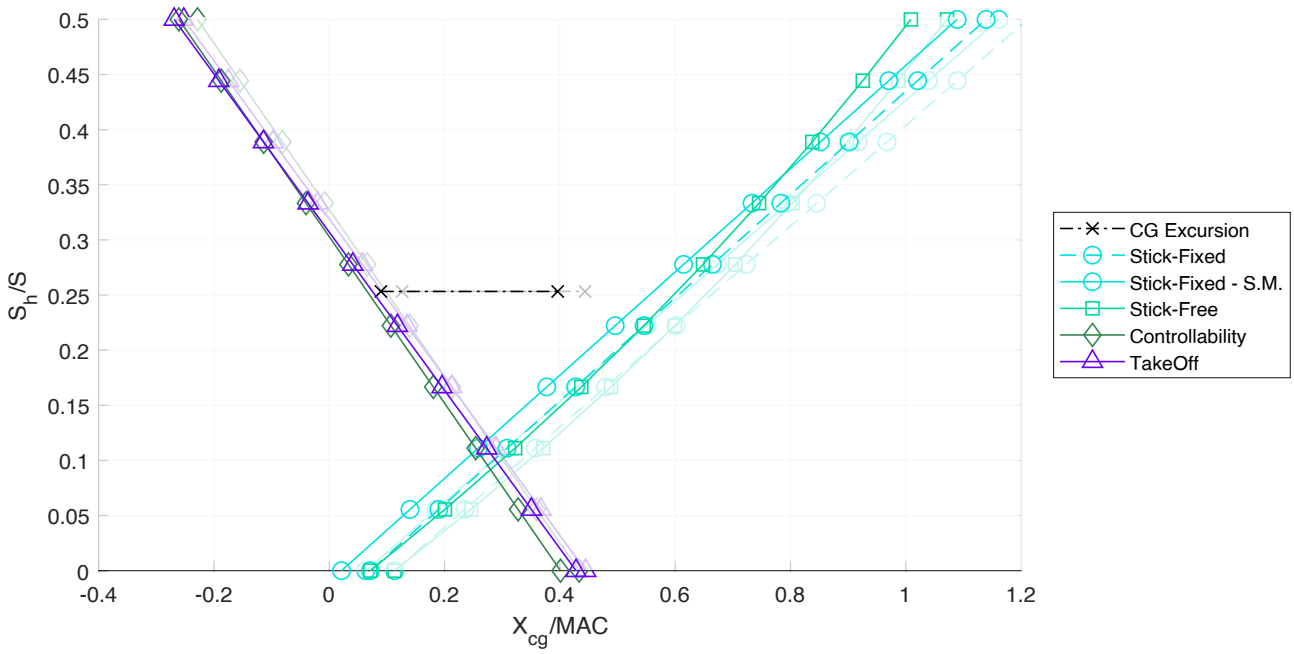

Figure 10 – Stability/controllability X-plot for change of BPR 4 to 14 for Case 1 (constant engine location)

Case 2:

Similar to the analysis for constant engine location, the analysis for constant spanwise location (see Figure 11) shows a forward shift of the graphs due to the forward shift of the CG. The forward CG limit is close to the limiting criteria and the CPR14 engine would in fact require a larger tail when the wing is not moved to meet the CG excursion limits. The change in aerodynamic center also causes a shift to the lift of all criteria.

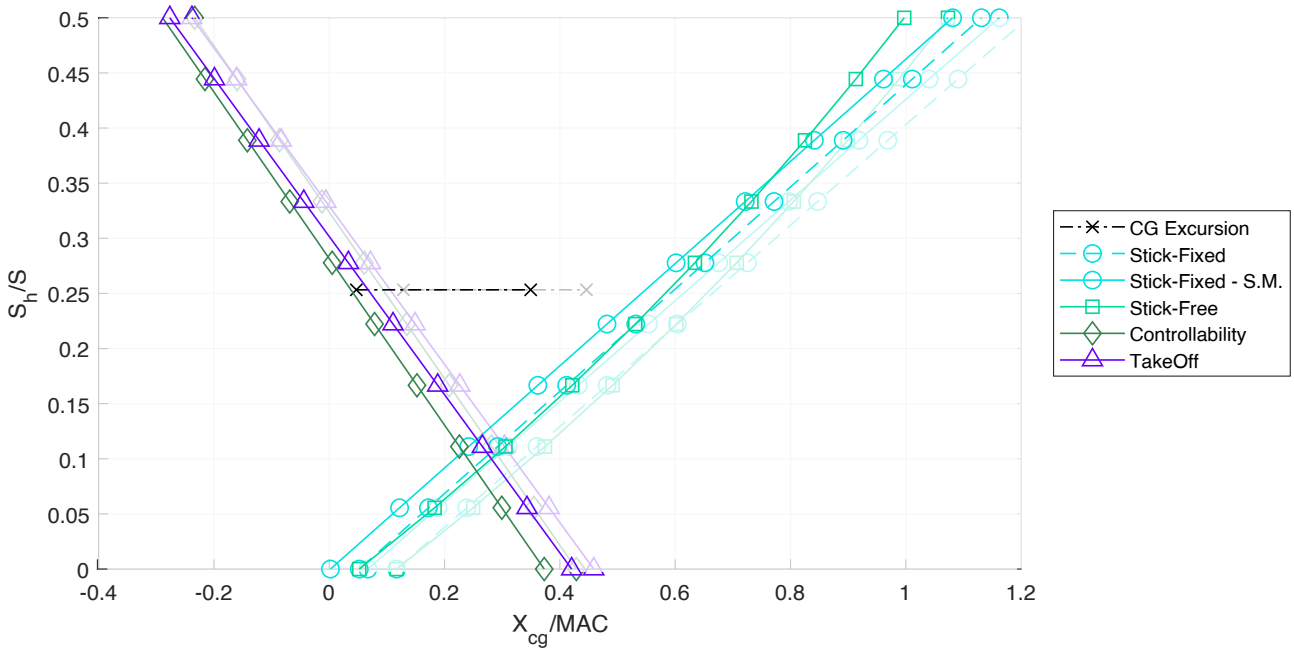

Figure 11 – Stability/controllability X-plot for change of BPR 4 to 14 for Case 2 (constant spanwise engine location)

Case 3:
Figure 12 illustrates the effect of variable engine location, showing the reduced margin and almost constant CG excursion. Consequently, the shift to the left is less, though still affected by the change in aerodynamic center location. This confirms the effect of engine size on aerodynamic center location (as concluded in sub-Section 4.1), as this effect is also dominant in all other cases. This can have an effect on the resulting required horizontal tail size as will be discussed in the next section.

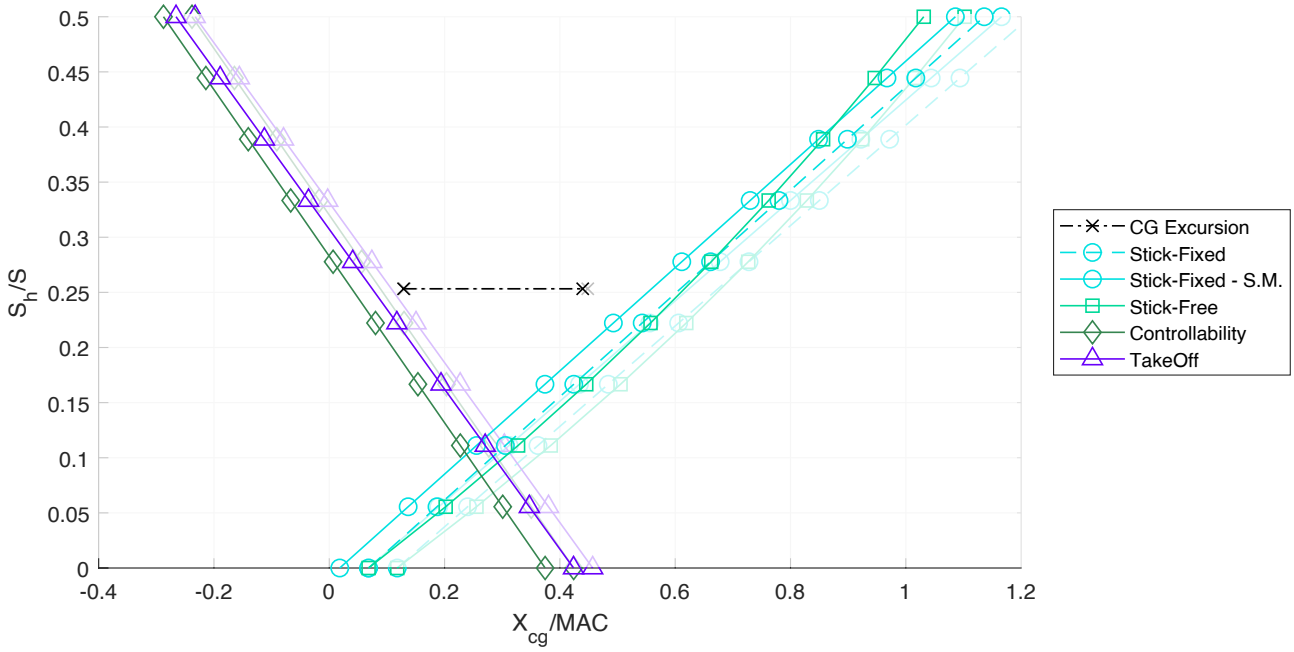

Figure 12 – Stability/controllability X-plot for change of BPR 4 to 14 for Case 3 (constant engine CG, variable location)

4.3 Combined results on horizontal tail size for retrofit

Figure 13 illustrates the combined results on the required horizontal tail size, also including the calculated tail size of the reference aircraft.

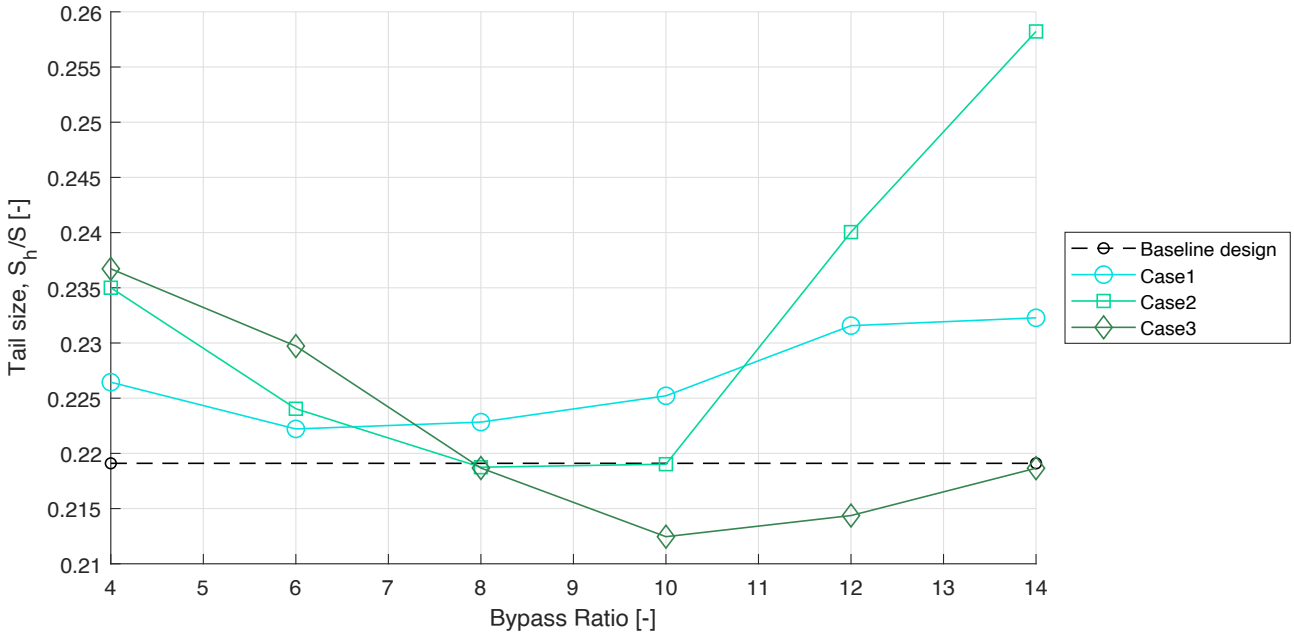

Figure 13 – Horizontal tail size for three engine location scenarios compared to the calculated A320 (engine based on A320 engine size) for a retrofit scenario

Where CG margins for all engine location cases show consistency, tail size does not. Case 1 requires the tail to increase by a maximum of 4.5% between BPR 6 and 14. For case 2 this is 18% between BPR 8 and 14. This can be explained from the individual stability plots, where forward CG location is limiting. Changes in aerodynamic center, C_{L_α}, and $C_{M_{AC}}$ cause the criteria to shift to the left. Compared to the baseline, the tail can be smaller. However, this is also affected by the family design of the A320. Similar reasoning can explain why for case 3 the tail size decreases. From Figure 12 it can be seen that the CG location is relatively stable while the criteria shift left. Hence, magnifying the effect of aerodynamic parameters. From BPR 10 onwards, the decreasing trend in tail size stagnates and actually reverses, indicating that a larger tail may be required for even larger BPR.

5. Results of aircraft resizing

The different engines with the different bypass ratio's and SFC as a inputs in the Initiator to perform a full aircraft design cycle. The engine dimensions corresponding to the various BPR were fixed in the input file. Other input parameters are based on an A320 type aircraft with constant payload and mission requirements. The top level requirements are provided in Table 2.

Table 2 – Top level requirements for the Airbus A320-200 used in the resizing analyses

Parameter	Value	Unit
Passengers	156	-
Maximum payload mass	20536	kg
Harmonic range	3917	km
Cruise Mach	0.78	-
Cruise altitude	11280	m
Take-off distance	1938	m
Landing distance	1480	m

The spanwise engine location was kept similar to location in the reference aircraft. The vertical location is kept constant as well, meaning the center line of the engine remains at the same place. Effectively, reducing the distance between engine and wing, as well as the ground clearance if the landing gear is not modified. Results of the aircraft resizing are shown in Figure 14, where the aircraft is completely resized in the Initiator for two different scenarios; (1) changing both SFC and engine size and weight on an airframe and (2) changing engine size and weight but keeping SFC constant.

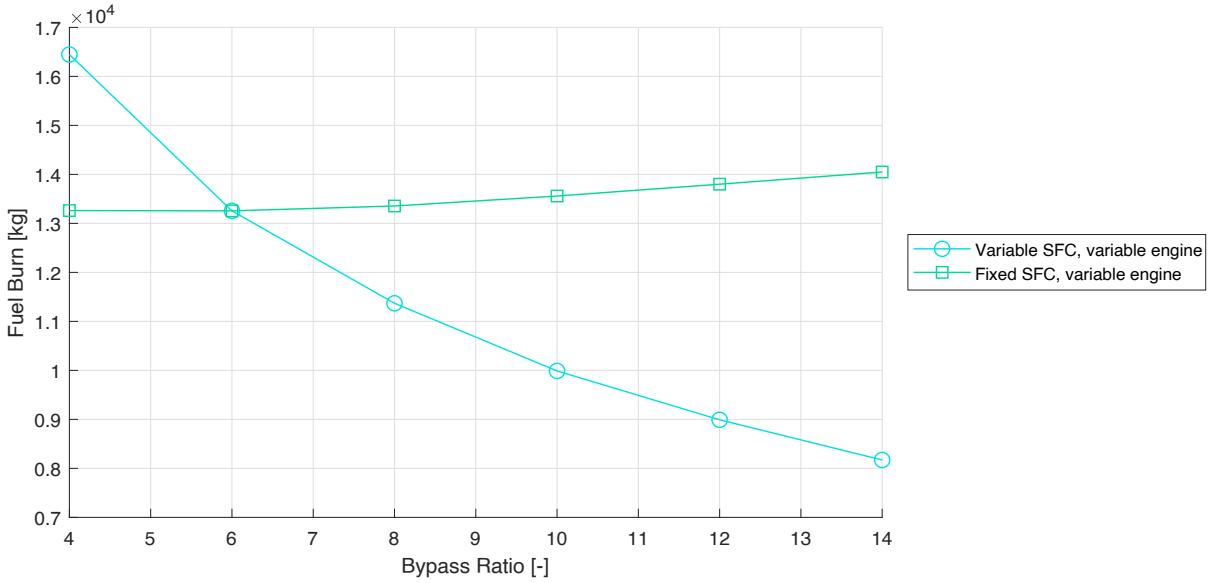

Figure 14 – Aircraft fuel burn for the different bypass ratio's, after a full aircraft redesign

The effect of the changing engine is minimal compared to the effect of the SFC. With the engine increasing in size (thus increasing the drag and increasing the weight), the overall increase in fuel burn is 5.9%. However, the decrease in fuel burn due when the SFC and engine effects are considered together, the fuel burn drops by 50%. In fact, the fuel burn curve directly follows the relation between SFC and BPR that is used.
When comparing the lifting surface of the aircraft, as presented in Figure 15, it can be seen that after BPR 10 there is little variation in the different surface areas. The decreasing fuel mass thanks to higher bypass ration is reducing MTOM and OEM, which is not affected significantly by the higher engine mass. After BPR 12, the horizontal tail area starts increasing again slightly, in line with the conclusions from the retrofit analysis.

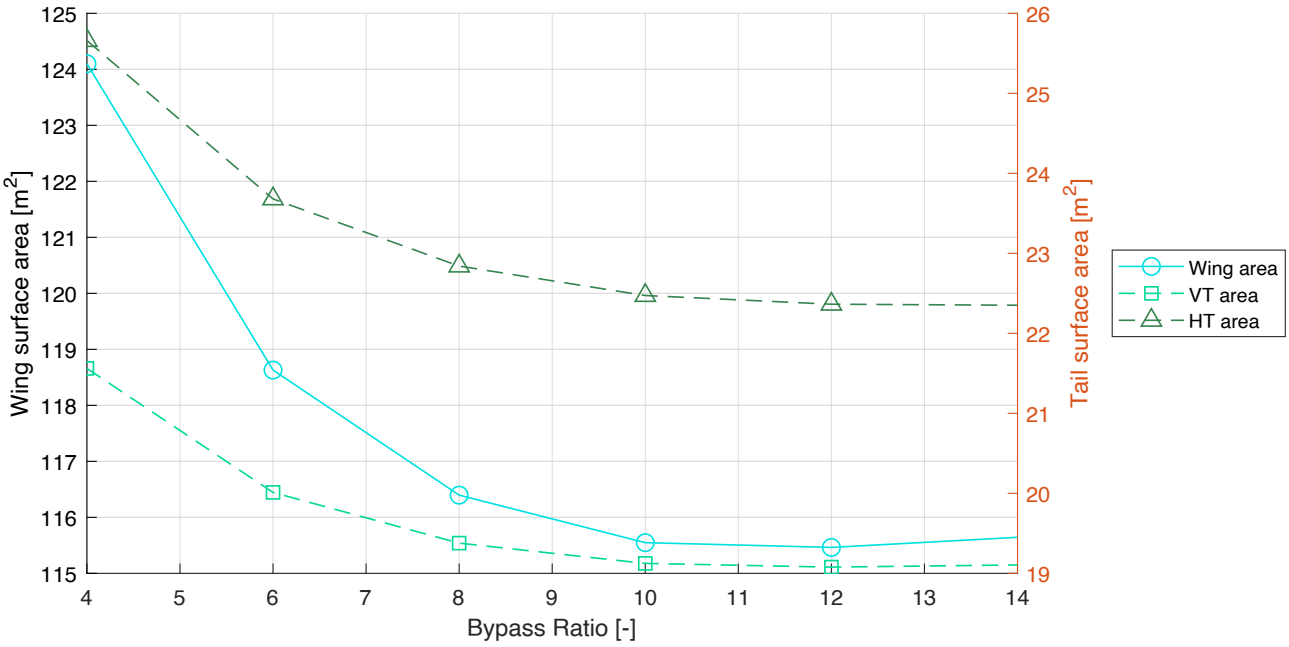

Figure 15 – Aircraft main wing and empennage surface areas after redesign

The reason why fuel burn decreases while OEM and wing surface area stay relatively constant, can be further explained when looking at wetted area. Aircraft wetted area is plotted against BPR in Figure 16.

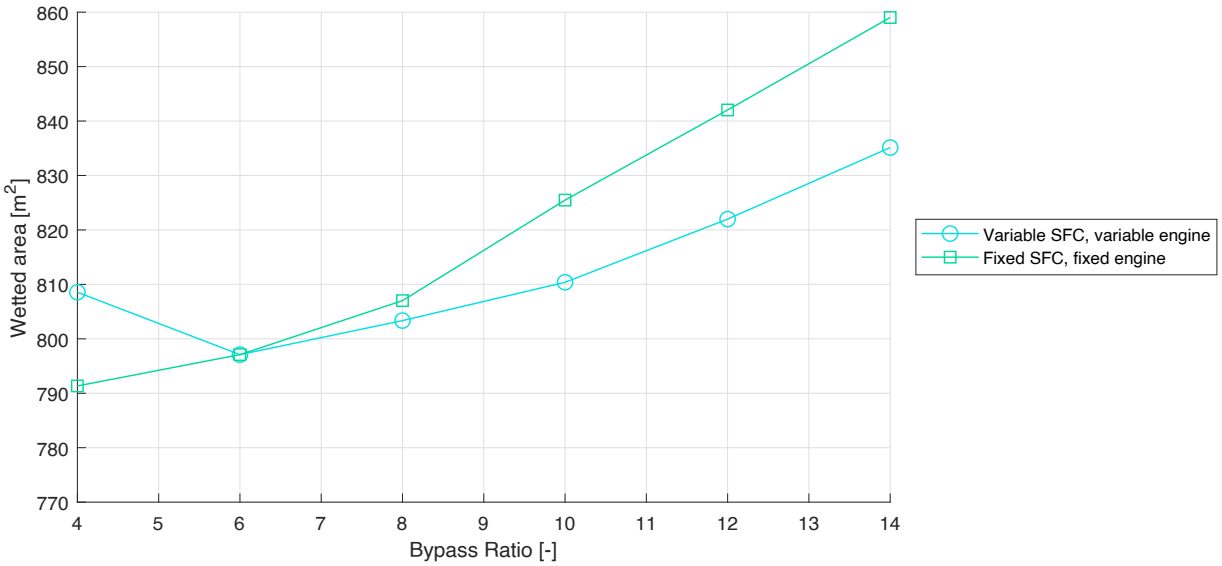

Figure 16 – Wetted area for different bypass ratios after redesign

This figure in fact shows an increase in wetted area. Since the wing and empennage do not increase in area, the reason is purely the larger nacelle due to the larger BPR, which will start to negatively affect the drag. The reduction in slope of fuel burn is likely caused by the increased drag due to the increased wetted area. The SFC of the engine itself still becomes better, even for larger BPR. The increased drag causes a decrease in performance gain. However, there is still a performance gain, even at larger BPR. For larger BPR, the location and the engine (nacelle) must be optimised for ground clearance. The reason for not further increasing the BPR lies in practical limitations such as mounting the engine under the wing of a low wing aircraft. The fan size also has limitations based on the fan tip velocity. This depends also on the fan shaft speed and other factors.

6. Conclusions

A variety of retrofit studies was performed, assessing the effects of engine location, BPR and combinations of these on aircraft stability/controllability. It can be concluded that engine size is more significant than its location. Changes in aerodynamic center, C_{L_α}, and $C_{M_{AC}}$ cause stability/controllability criteria to shift to the left. Depending on the way a larger engine is fitted, an effect will be visible in CG excursion. With heavier engines at the same spanwise location, causing a more forward CG location that may become limiting for a retrofit. Whereas the CG margins for all the engine location cases showed some consistency, the tail size is less consistent. From BPR 10 onwards, the decreasing trend in tail size stagnates and actually reverses, indicating that larger tail sizes might be required for even larger BPR engines.

The effect of the changing engine dimension is minimal compared to the effect of the SFC when assessing an aircraft redesign around the new engine. Using the Initiator toolbox it was found that lower fuel burn, due to SFC improvements, always resulted in a lighter aircraft for a given mission. With the engine increasing in size (thus increasing the drag and increasing the weight), the overall increase in fuel burn is 5.9%. However, the decrease in fuel burn due when the SFC and engine effects are considered together, the fuel burn drops by 50%. The reduction in fuel burn negates the increase in engine weight, drag, and integration issues. The calculated maximum increase in tail size was found to be 18%. Compared to the baseline aircraft tail size, it is only a 2% increase at maximum. This result is slightly obscured due to the fact that for the reference aircraft, an Airbus A320 is considered, whose tail plane is in fact designed for the entire family of aircraft.

Contact Author Email Address

Maurice Hoogreef m.f.m.hoogreef@tudelft.nl

Acknowledgements

The work presented in this article is based on the MSc thesis by T.E. Boogaart, [4]. The authors would like to acknowledge Dr. Vivek Ahuja from Research in Flight and Prof. dr. Roy Hartfield from Auburn University for their guidance and assistance during the FlightStream analyses that were performed to generate results presented in this paper.

Copyright Statement

References

[1] ANONYMOUS. Flightpath 2050: Europe's vision for aviation: Report of the high level group on aviation research, 2011.

[2] ARDEMA, M. D., CHAMBERS, M. C., PATRON, A. P., HAHN, A. S., MIURA, H., AND MOORE, M. D. Analytical fuselage and wing weight estimation of transport aircraft. Tech. Rep. TM 110392, National Aeronautics and Space Administration, May 1996.

[3] BERRY, D. L. The boeing 777 engine/airframe integration aerodynamic design process. In *ICAS 1994* (1994), vol. 19, AMERICAN INST OF AERONAUTICS AND ASTRONAUTICS, pp. 1305–1305.

[4] BOOGAART, T. Evaluation of the overall installation penalty of aero-engines for single aisle aircraft: A comparison between engine retro-fit and aircraft redesign. Master's thesis, Delft University of Technology, 2021.

[5] COVERT, E. D. Thrust and drag: Its prediction and verification. *AIAA Progress in Astronautics and Aeronautics 98* (1985), 317–330.

[6] ELMENDORP, R. J. M., AND LA ROCCA, G. Comparitive design & sensitivity studies on box-wing airplanes. In *Italian Association of Aeronautics and Astronautics - XXV International Congress* (2019).

[7] ELMENDORP, R. J. M., VOS, R., AND LA ROCCA, G. A conceptual design and analysis method for conventional and unconventional airplanes. In *ICAS 2014: Proceedings of the 29th Congress of the International Council of the Aeronautical Sciences, St. Petersburg, Russia, 7-12 September 2014* (2014), International Council of Aeronautical Sciences.

[8] GODARD, J. L., HOHEISEL, H., ROSSOW, C.-C., AND SCHMITT, V. Investigation of interference effects for different engine positions on a transport aircraft configuration. In *DLR Workshop Braunschweig* (1996).

[9] GUYNN, M., BERTON, J., FISHER, K., HALLER, W., TONG, M., AND THURMAN, D. Analysis of turbofan design options for an advanced single-aisle transport aircraft. In *9th AIAA Aviation Technology, Integration, and Operations Conference (ATIO) and Aircraft Noise and Emissions Reduction Symposium (ANERS)* (2009), p. 6942.

[10] HOERNER, S. F. Fluid-dynamic drag. *Hoerner fluid dynamics* (1965).

[11] HOHEISEL, H. Aerodynamic aspects of engine-aircraft integration of transport aircraft. *Aerospace science and technology 1*, 7 (1997), 475–487.

[12] HOOGREEF, M. F. M., DE VRIES, R., SINNIGE, T., AND VOS, R. Synthesis of aero-propulsive interaction studies applied to conceptual hybrid-electric aircraft design. In *AIAA Scitech 2020 Forum, Orlando, Florida, USA* (2020).

[13] HOOGREEF, M. F. M., VOS, R., DE VRIES, R., AND VELDHUIS, L. L. M. Conceptual assessment of hybrid electric aircraft with distributed propulsion and boosted turbofans. In *AIAA Scitech 2019 Forum* (2019), p. 1807.

[14] JDIOBE, M., HICKMAN, K., KIDD, J. A., AND FALA, N. Improving undergraduate aerospace engineer professional readiness through boeing 737 max crash case study. In *AIAA AVIATION 2020 FORUM* (2020), p. 2937.

[15] PFLUG, M., AND HABERLAND, C. On numerical jet flow simulation of current and future high by-pass engines. *Aspects of engine airframe integration for transport aircraft* (1996), 25–1.

[16] RIVERS, M. B., AND DITTBERNER, A. Experimental investigations of the nasa common research model. *Journal of Aircraft 51*, 4 (2014), 1183–1193.

[17] ROBINSON, M., MACMANUS, D. G., AND SHEAF, C. Aspects of aero-engine nacelle drag. *Proceedings of the Institution of Mechanical Engineers, Part G: Journal of Aerospace Engineering 233*, 5 (2019), 1667–1682.

[18] RUDNIK, R., ROSSOW, C.-C., AND GEYR, H. F. V. Numerical simulation of engine/airframe integration for high-bypass engines. *Aerospace Science and Technology 6*, 1 (2002), 31–42.

[19] TINOCO, E. N., BRODERSEN, O. P., KEYE, S., LAFLIN, K. R., FELTROP, E., VASSBERG, J. C., MANI, M., RIDER, B., WAHLS, R. A., MORRISON, J. H., HUE, D., ROY, C. J., MAVRIPLIS, D. J., AND MURAYAMA, M. Summary data from the sixth aiaa cfd drag prediction workshop: Crm cases. *Journal of Aircraft 55*, 4 (2018), 1352–1379.

[20] TORENBEEK, E. *Synthesis of subsonic airplane design*. Delft University Press, 1982.

[21] VOS, R., AND FAROKHI, S. *Introduction to transonic aerodynamics*, vol. 110. Springer, 2015.

[22] VOS, R., AND HOOGREEF, M. F. M. Semi-analytical weight estimation method for fuselages with oval cross-section. In *54th AIAA/ASME/ASCE/AHS/ASC Structures, Structural Dynamics, and Materials Conference* (2013), p. 1719.

[23] VOS, R., AND HOOGREEF, M. F. M. System-level assessment of tail-mounted propellers for regional aircraft. In *Proceedings of the 31st Congress of the International Council of Aeronautical Sciences* (2018).